Talanta 207 (2020) 120298

Contents lists available at ScienceDirect

Talanta

journal homepage: www.elsevier.com/locate/talanta

A ratiometric electrochemical DNA biosensor for detection of exosomal MicroRNA

Lipei Luo[a,1], Liangliang Wang[b,1], Lupeng Zeng[b], Yuru Wang[b], Yunping Weng[b], Yijuan Liao[c], Tingting Chen[b], Yaokun Xia[b], Jing Zhang[c,**], Jinghua Chen[b,*]

[a] Department of Pharmacy, The Second Affiliated Hospital of Fujian Medical University, Quanzhou, Fujian Province, 362000, PR China
[b] Department of Pharmaceutical Analysis, The School of Pharmacy, Fujian Medical University, Fuzhou, Fujian Province, 350122, PR China
[c] College of Life Sciences, Fujian Agriculture and Forestry University, Fuzhou, Fujian Province, 350002, PR China

ARTICLE INFO

Keywords:
Exosomal microRNA
Ratiometric electrochemical DNA biosensor
Locked nucleic acid
Strand displacement reaction

ABSTRACT

The detection of exosomal microRNAs (miRNAs) derived from cancer cells with sensitive and selective methods has stimulated increasing interest due to its potential utility in the application of tumor diagnosis. Here, we developed a ratiometric electrochemical DNA biosensor based on a locked nucleic acid (LNA)-modified "Y" shape-like structure for the detection of exosomal miRNA-21 (miR-21). When miR-21 is present, the LNA-assisted strand displacement reaction on the "Y" shape-like structure is activated, leading to a structure change and augmentation of the signal ratio, which reflects the different distances between the electrode surface and two electroactive molecules labeled on the "Y" shape-like structure. With this dual signal ratiometric method, the biosensor shows high accuracy and sensitivity with a limit of detection as low as 2.3 fM. Moreover, because of the logarithm of the signal ratio displays a linear relationship with the logarithm of the miR-21 concentration, the biosensor is stable enough to be used in the detection of miR-21 in MCF-7 cell-derived exosomes. In addition, the biosensor shows good selectivity even in the detection of even a single base-mismatched target due to the LNA-assisted strand displacement reaction. Notably, the sensor is both regenerative and robust. In brief, the high sensitivity and selectivity, combined with the low cost of the glassy carbon electrode, make this biosensor a promising tool for the development of point-of-care testing in cancer.

1. Introduction

Exosomes are microvesicles with a diameter of 50–200 nm derived from multivesicular body pathways [1,2], that are involved in many physiological and pathological processes [3–5]. Importantly, a large amount of the cargo of exosomes, such as proteins [6], lipids [7], microRNAs (miRNAs) [8,9] and mRNAs [10], play crucial roles in exosomes functions. Particularly, miRNAs, a collection of endogenous non-coding single-stranded RNAs of 19–23 nucleotides, can affect gene expression by inhibiting translation or cleavage upon binding to the 3′ untranslated regions or open reading frames of the target mRNAs [11,12]. Recently, exosomal miRNAs (eg. miR-21, miR-146, miR-203) were reported to be highly specific in tumorigenesis, tumor progression and metastasis [13–16]. The lipid bilayer of exosomes effectively protects miRNAs from enzymes degradation, increasing their stability and abundance. Thus, exosomal miRNAs have great potential to serve as tumor biomarkers for clinical diagnosis, treatment and prognosis. An important endeavor involves the development of a simple, reliable and sensitive method for detecting the level of specific exosomal miRNAs.

Conventional miRNA detection methods include northern blotting [17], reverse transcription-polymerasechain reaction (RT-PCR) [18], and microarray analysis [19]. These methods have been successfully used for miRNA quantification, while some issues, such as those involving the complex preprocessing pipeline and relatively high labor costs, have hindered their further application. In recent years, a multitude of approaches based on microfluidic [20], localized surface plasmon resonance [21], surface-enhanced Raman scattering [22,23], and fluorescence [24–26] have been devoted to detecting exosomal miRNAs by means of individual superiorities. Additionally, a few electrochemical biosensors have been used due to the advantages of simple operation, high sensitivity, fast analysis speed, low cost and easy miniaturization [27–29]. For instance, Pang et al. have constructed a

* Corresponding author.
** Corresponding author.
E-mail addresses: 1601225385@qq.com (J. Zhang), cjh_huaxue@126.com (J. Chen).
[1] Authors with equal contributions.

https://doi.org/10.1016/j.talanta.2019.120298
Received 28 April 2019; Received in revised form 20 August 2019; Accepted 24 August 2019
Available online 26 August 2019
0039-9140/

visible light-driven self-powered device for the quantification of serum-derived exosomal miRNA [30]; Boriachek et al. have proposed an amplification-free electrochemical approach for the detection of cancer-derived exosomal miR-21 [31]; and Tavallaie et al. have designed rational nucleic acid hybridization methods based on an electrically reconfigurable network of gold-coated magnetic nanoparticles, achieving miRNA detection of blood exosomes [32]. However, these electrochemical methods only involve single signals, which could easily be subject to experimentally- and environmentally-associated signal drifting. Notably, some electrochemical biosensors have been combined with ratiometric methods [33,34] to impact a self-referencing/calibration property, which helps reduce the false-positive/negative signal. Benefiting from the ratiometric readout, in our previous study, our group developed a ratiometric electrochemical DNA biosensor based on the signal cascade amplification of DNA for exosomal miR-21 detection with high accuracy and sensitivity [35]. Though this method greatly improved the detection of exosomal miRNA, its practicality was limited in that it still involved multiple DNA probes and a relatively complicated strand displacement process.

Herein, we describe our development of an amplification-free ratiometric electrochemical biosensor based on simple transformation of a "Y" shape-like structure mediated by a locked nucleic acid (LNA)-assisted strand displacement reaction (LSDR) for exosomal miR-21 detection. In the presence of miR-21, the LSDR occurred, and the "Y" shape-like structure transformed into a hairpin structure, which turned the methylene blue (MB) signal on and ferrocene (Fc) signal off. Through the change in the current ratio of MB and Fc, sensitive electrochemical detection for exosomal miR-21 with a limit of detection (LOD) of 2.3 fM was realized. Furthermore, the modification of the LNA increased the stability and efficiency of the strand displacement reaction by increasing the melting temperature of the DNA duplex, which enhanced the differentiation ability of base mismatching [36]. The electrochemical biosensor together with the ratiometric readout has excellent analytical performance with good reproducibility and high sensitivity and reliability, suggesting future promise for the development of point-of-care testing in cancer.

2. Experimental methods

2.1. Reagents and apparatus

HPLC-purified miRNAs and all DNA oligonucleotides were synthesized by Takara Biotechnology Co., Ltd. (Dalian, China), and their base sequences are shown in Table S1. Fetal bovine serum (FBS), Roswell Park Memorial Institute medium (RPMI), phosphate buffer solution (PBS) and penicillin-streptomycin solution were purchased from Hyclone. Exosomal protein lysis buffer was purchased from Weihui Biotechnology Co., Ltd (Beijing, China). Radio immunoprecipitation assay (RIPA) lysis buffer was purchased from Beyotime Biotechnology Co., Ltd. The Bicinchoninic Acid (BCA) Protein Assay Kit was purchased from Thermo Fisher Scientific. Sodium dodecyl sulfate-polyacrylamide gel electrophoresis (SDS-PAGE) gel preparation kit, paraformaldehyde and glutaraldehyde were purchased from Solarbio Sciences & Technology Co., Ltd (Beijing, China). Polyvinylidene fluoride membranes (PVDF) were purchased from Dingguo Changsheng Biotechnology Co., Ltd (Beijing, China). Tris buffered saline (TBS) and Tween 20 were purchased from Sangon Biotech Co., Ltd (Shanghai, China). Ago2 antibody, TSG101 antibody, CD63 antibody and secondary antibody were purchased from Abcam. Exosomes antibodies, array & enzyme-linked immunosorbent assay (ELISA) kit were purchased from System Biosciences (SBI). TRIzol was purchased from Beyotime Biotechnology Co., Ltd. MiScript II RT Kit and miScript SYBR Green PCR Kit were purchased from Qiagen. 1-ethyl-3-(3- dimethylaminopropyl) carbodiimide hydrochloride (EDC) and N-hydroxysuccinimide (NHS) were analytical grade and were purchased from Sigma. All the other chemicals were analytical grade and purchased from Sinopharm Chemical Reagent Co., Ltd (Shanghai, China). All aqueous solutions were prepared with Milli-Q water (18 MΩ). Human breast cancer cell line MCF-7 was purchased from China Center for Type Culture Collection in Shanghai.

The ultracentrifuge was Beckman Optima XPN-100 (Beckman, USA). Transmission electron microscopy (TEM) images were visualized on a JEM-2010 microscope (JEOL Ltd., Japan). The dynamic light scattering (DLS) was carried out by Litesizer 500 (Anton Paar, Austria). The images of proteins were collected by the Bio-Rad ECL detection system (Bio-Rad, USA). RT-qPCR was implemented and analyzed with MxPro-MX3000P software (Agilent Technologies, USA). Differential pulse voltammetry (DPV) and electrochemical impedance spectroscopy (EIS) measurements were assessed on a CHI660E analyzer (Shanghai Chenhua Instrument Co., Ltd, China).

2.2. Cell culture and exosomes isolation

MCF-7 cells were cultured in RPMI containing 10% FBS, 1% penicillin and streptomycin. MCF-7 cells (1×10^8 cells) were cultured in FBS-free RPMI for 48 h before exosomes isolation. Then exosomes were isolated from the cell culture supernatants by ultracentrifugation. Briefly, the cell culture medium was firstly centrifuged at 300 g for 10 min and then 2000 g for 15 min to remove intact cells, dead cells and cell debris. Finally, the supernatant was centrifuged at 100,000 g for 70 min to acquire exosomes, which were then washed, resuspended in PBS and stored for later use at −80 °C.

2.3. Exosomes quantification by ELISA

Firstly, the isolated exosomes were added into the microtiter plate provided in Exosomes antibodies, array & ELISA kit, and incubated at 37 °C overnight. After three rinses, specific rabbit anti-human CD63 antibody (System Biosciences) was added and the plates were incubated for 1 h at room temperature. Then, the plates were washed and incubated with HRP-conjugated goat anti-rabbit antibody (SBI) for 1 h. After a final wash, a reaction was performed with sensitive 3, 3′, 5, 5′-tetramethylbenzidine (TMB) substrate followed by blocking with a stop buffer. Finally, the optical densities were recorded at 450 nm using a Multiskan GO microplate spectrophotometer (Thermo Fisher Scientific, U.S.A.).

2.4. Transmission electron microscopy

Five microliters of an equal volume mixture of purified exosomes in PBS and 4% paraformaldehyde were placed onto the surface of a copper mesh for 20 min. Then, exosomes were fixed in 4% glutaraldehyde for 5 min, and washed three times with deionized water. Filter paper was used to blot excess water, and the exosomes were stained for 5 min with 1% uranyl acetate. After drying at room temperature, the samples were observed on a JEM-2010 microscope (JEOL Ltd., Japan).

2.5. Dynamic light scattering

The effective hydrodynamic diameters of exosomes derived from MCF-7 cells were measured with a Litesizer 500 (Anton Paar, Austria) equipped with a 35 mW laser diode light ($\lambda = 658$ nm), and the scattered light at an angle of 90° was measured. Samples were diluted with filtered PBS to 1 mL, and then they were transferred to solvent-resistant cuvettes for light scattered measurement at a fixed position. The target temperature was controlled at 25 °C.

2.6. Western blotting analysis of exosomal proteins

The proteins of MCF-7 cells and exosomes were extracted in RIPA lysis buffer and exosomal proteins lysis buffer, respectively. Then a BCA Protein Assay Kit was used to quantify the total proteins concentration. Firstly, a mixture of the proteins and the loading buffer was boiled at

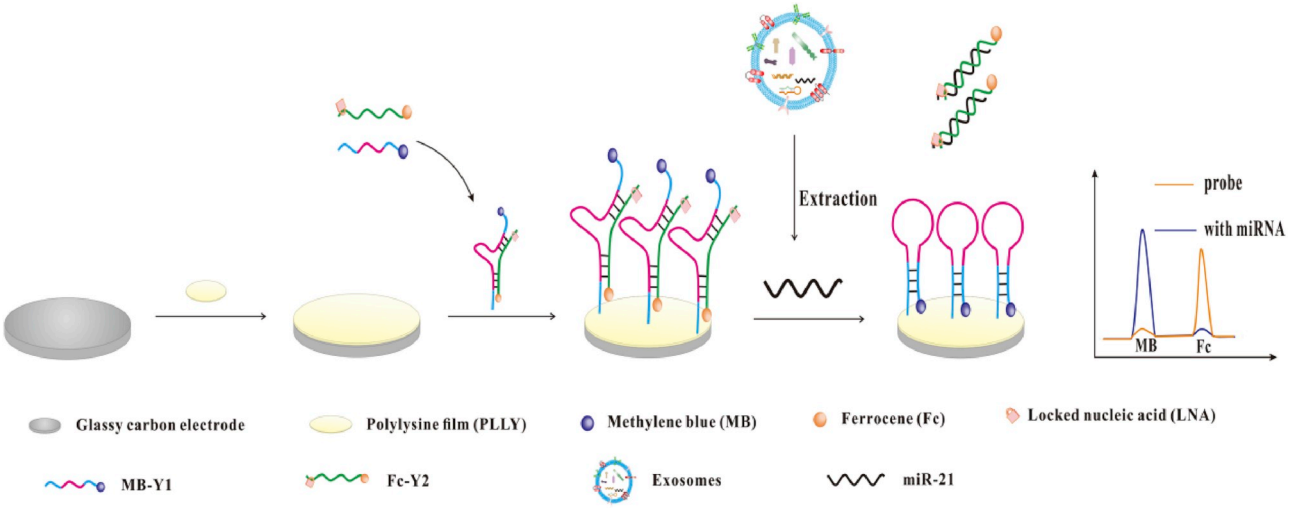

Fig. 1. Schematic illustration of the ratiometric electrochemical biosensor for exosomal miR-21 detection.

95 °C for 5 min. Then, the exosomal proteins were separated by 12% SDS-PAGE at 80 V for 30 min and 100 V for 1 h. Subsequently, the proteins were transferred to PVDF pre-activated by methanol in transfer buffer (25 mM Tris, 192 mM glycine, 20% methanol) at 300 mA for 1 h. After blocking for 2 h with 5% non-fat powdered milk dissolved in TBST (TBS + Tween 20) buffer, the PVDF membranes were incubated with 200 μL of Ago2 antibody, TSG101 antibody or CD63 antibody solution overnight at 4 °C. Next, the blots were incubated with secondary antibody (Abcam, USA) for 1 h at room temperature. Finally, the immune-reactive bands were visualized with an enhanced chemiluminescence reagent (Thermo Fisher Scientific, USA), and the images were obtained from an ECL detection system (Bio-Rad, USA).

2.7. RT-qPCR analysis of miR-21

Firstly, total RNA derived from exosomes (3.42×10^{11} particles/mL) was extracted in TRIzol reagent according to the manufacturer's protocol and quantified on a NanoDrop ND-2000 (Thermo Scientific). Then, total RNA was converted to cDNA using a miScript II RT Kit. The reactions were carried out at 37 °C for 1 h, and then 95 °C for 5 min. Next, PCR was performed using the miScript SYBR Green PCR Kit. The protocol for the thermocycler was as follows: 95 °C for 15 min, followed by 50 cycles of 94 °C for 15 s, 55 °C for 30 s, and 70 °C for 30 s. The PCR reaction was carried out with U6 as an internal reference on an Mx3000P machine (Agilent Technologies, USA), and threshold cycle (Ct) data were collected with MxPro-Mx3000P software.

2.8. Electrode pretreatment and probe assembly

The glassy carbon electrode (GCE) was firstly polished with 0.3 μm and 0.05 μm Al_2O_3 water solution and then ultrasonically cleaned with ethanol and distilled water for 5 min each. Next, the surface of the electrode was dipped in 5 mM $[Fe(CN)_6]^{3-}$ (containing 0.01 M KCl), rinsed with deionized water, and dried with flowing nitrogen. The electrode was then dipped in 0.2 M PBS containing 0.01 M lysine for modification of the polylysine membrane (PLLy/GCE) by cyclic voltammetry essentially as described [37]. The conditions were as follows: a voltage range of −1.0- +2.4 V, a scanning rate of 100 mV/s, and 14 scan cycles. Subsequently, 20 μL of coupling activator (5 mM EDC and 8 mM NHS in phosphate buffer, pH 7.4) were added to the surface of the modified electrode for 60 min at room temperature, and the electrode was rinsed with deionized water, and dried with flowing nitrogen. Finally, 10 μL mixed solution of MB-modified Y1 DNA probe (MB-Y1) and Fc-modified Y2 DNA probe (Fc-H2) was dropped on the surface of the above-activated electrode. After being rinsed and dried, the probe-assembled electrode of MB-Y1/Fc-Y2/PLLy/GCE was set aside for later use.

2.9. Electrochemical detection of miR-21

MiR-21 solutions (10 μL) of different concentrations were firstly dispensed onto the surface of MB-Y1/Fc-Y2/PLLy/GCE for 90 min at room temperature, rinsed with ultrapure water and blown dry with flowing nitrogen. Then, the electrodes were placed in EIS detection buffer (containing 0.02 M $K_4Fe(CN)_6$, 0.02 M $K_3Fe(CN)_6$, 10 mM Tris and 0.1 M KCl, pH 7.0) to measure the impedance of the differently modified electrodes. The EIS parameters were set as follows: an initial potential of 0.21 V (versus Ag/AgCl), an amplitude width of 0.005 V and a frequency range of 0.1 Hz–10^5 Hz. DPV curves were scanned in PBS solution. The conditions of measurement were as follows: a sweep potential range of −0.4 V to +0.6 V, a potential increment of 0.005 V, an amplitude width of 0.025 V and a frequency of 10 Hz.

3. Results and discussion

3.1. Detection mechanism of the ratiometric electrochemical biosensor

The ratiometric electrochemical DNA biosensor was constructed and applied to the detection of exosomal miR-21. As shown in Fig. 1, firstly, a layer of PLLy was electropolymerized on the GCE surface, forming PLLy/GCE and providing abundant bonding sites for carboxyl. Next, a mixture solution of MB-Y1 modified with MB and amino group and Fc-Y2 modified with Fc and LNA was dropped on the PLLy/GCE. In the mixture solution, MB-Y1 was firstly hybridized with Fc-Y2 to form a "Y" shape-like DNA structure, and then the structure was immobilized on PLLy/GCE through the amido linkage. Here, the MB was far away from the electrode interface and the Fc was introduced to the electrode interface, generating a weak current signal of MB (I_{MB}) and an obvious current signal of Fc (I_{Fc}). According to our design, miR-21 could hybridize complementarily with the Fc-Y2 DNA probe via a LSDR. Consequently, the Fc-Y2 DNA probe would dissociate from the MB-Y1 chain, causing MB-Y1 to fold into a hairpin structure. Thus, Fc would be released from the electrode interface and MB would be close to the electrode interface, which would induce a decrease in I_{Fc} and an increase in I_{MB}. Conversely, when miR-21 was absent, there would be no structural transformation on the electrode interface, accompanied by a weak signal of MB and a strong signal of Fc. Finally, sensitive detection of exosomal miR-21 would be achieved by recording the ratio changes of the two indicator current signals before and after the addition of exosomal miR-21.

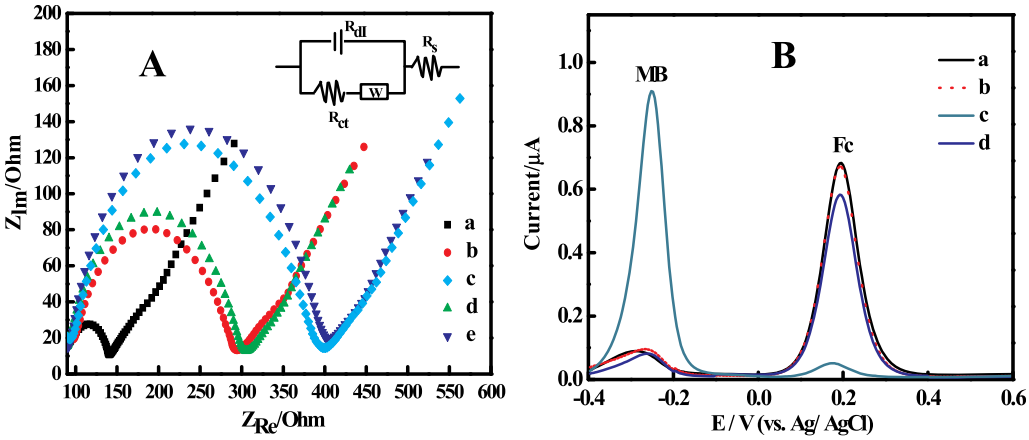

Fig. 2. A. Electrochemical impedance spectroscopy (EIS) of different modified glassy carbon electrodes. a) PLLY/GCE; b) Y1/PLLY/GCE; c) Y2-Y1/PLLY/GCE; d) miR-21 + Y2/Y1/PLLY/GCE; e) d + Y2. Inset: the EIS equivalent circuit plot. B. Differential pulse voltammetry curves of "Y" probe-modified glassy carbon electrodes (a) and after the addition of buffer (b) or miR-21(c) and regeneration (d).

3.2. Feasibility characterization of the biosensor

The electrode assembly process was firstly characterized by EIS. After measurement, the EIS equivalent circuit was simulated using the randle method (Fig. 2A Inset). And then, a Nyquist plot of the circuit was fitted with Z_{Im} versus $Z_{Re.}$ As depicted in Fig. 2A, the Nyquist plot of the modified glassy carbon electrode (PLLy/GCE, curve a) had a wide linear range and a small semicircle diameter with an electron transfer resistance (R_{ct}) of 50 Ω, indicating a very fast electron transfer process controlled by the diffusion effect. After the Y1 DNA probe was assembled to the electrode surface (Y1/PLLy/GCE, curve b), the R_{ct} increased to 197 Ω because of a repelling effect between the negatively charged $[Fe(CN)_6]^{3-/4-}$and the phosphoric acid skeletons. Upon the addition of Y1 and Y2 DNA probes (Y2-Y1/PLLy/GCE, curve c), the R_{ct} persistently increased to 306 Ω. Because the number of DNA phosphate skeletons on the electrode surface increased, the repulsion force to $[Fe(CN)_6]^{3-/4-}$ was enhanced, and the resistance of electrons transfer increased. In the presence of miR-21 (miR-21 + Y2/Y1/PLLY/GCE, curve d), R_{ct} was significantly reduced to 216 Ω owing to the complete complementary pairing of miR-21 with the Y2 probe, which led to a decrease in the number of DNA phosphate skeletons with a negative charge on the electrode surface, weakened the repulsion force of $[Fe(CN)_6]^{3-/4-}$ and reduced R_{ct}. When the Y2 probe was continuously added (d + Y2, curve e), R_{ct} increased to the vicinity (314 Ω) of the curve c, indicating that Y1 could continue to hybridize with Y2 to form a "Y" shape-like structure. The EIS results support the assembly process of the electrode. Importantly, the combination of curve c, d, and e indicate that the biosensor was reproducible.

Next, the electrode assembly process was further characterized by DPV. The results are shown in Fig. 2B. After the immobilization of the "Y" shape-like structure on the electrode surface, the electrode signal of the MB site was weak at the negative potential and the electrode signal of the Fc site was strong at the positive potential (black curve, a). When buffer as a blank control was added to the surface of the assembled electrode, the pattern of DPV (red dotted curve, b) was consistent with curve a. After miR-21 solution was added, the MB signal at the negative potential of the electrode signal was enhanced and the Fc signal at the positive potential was weakened (green curve, c). Finally, when re-adding Fc-Y2 in the above electrode surface (c + Fc-Y2), the "Y" shape-like structure reformed, leading to a weakened signal of MB and an enhanced signal of Fc (blue curve, d). The above results are in accordance with those of EIS, further confirming the feasibility of this biosensor.

3.3. Optimization of experimental conditions

In order to achieve a better performance, experimental conditions (such as the MB-Y1 concentration, pH and reaction time) affecting the whole sensing procedure were optimized. Firstly, the MB-Y1 concentration was examined as shown in Fig. S1A. In the range of 1–10 μM, the I_{MB}/I_{Fc} value increased with increasing Y1 concentration and reached a maximum at a concentration of 5 μM. Next, the pH of the buffer was varied as shown in Fig. S1B. As the pH value increased, the I_{MB}/I_{Fc} value firstly increased gradually before decreasing and reached a maximum at pH 8. The reaction time of miR-21 and Y2-Y1/PLLy/GCE was also examined as shown in Fig. S1C. The I_{MB}/I_{Fc} value firstly increased with increasing reaction time, reaching a maximum at 1.5 h and then remaining steady. Finally, the optimum concentration of the MB-Y1 probe was 5 μM, the optimum pH was 8.0 and the optimum reaction time was 1.5 h.

3.4. The sensitivity of the biosensor

Using the above optimal experimental conditions, electrodes were inserted into a series of miR-21 solutions with different concentrations. Then, the DPV responses of the two electrochemical signals from the electrodes were scanned and the I_{MB}/I_{Fc} value was used to evaluate the sensitivity. The results are shown in Fig. 3A and Fig. 3B, respectively. When the concentration of miR-21 increased, the I_{MB} gradually increased at the negative potential and the I_{Fc} gradually decreased at the positive potential. As seen in Fig. 3C, in the range of 10–70 fM, the logarithm of I_{MB}/I_{Fc} showed a good linear relationship with the logarithm of the miR-21 concentration, which is better than the result measured by square wave voltammetry (SWV) (Fig. S2). The linear regression equation was $\log (I_{MB}/I_{Fc}) = 2.7769 \mathrm{Log} C_{miR\text{-}21} - 3.7825$, with a correlation coefficient (r) of 0.9944 and a LOD of 2.3 fM. When compared with most of amplification-free methods for the detection of exosomal miRNAs (Table S2), our biosensor has comparable or higher sensitivity. Though its sensitivity is not as good as some microfluidic, SERS, and signal amplification strategy-based methods (Table S2), our biosensor is simpler, more cost-effective, and more compact. The determination of 50 fM miR-21 was repeated 8 times, and the results show that the relative standard deviation (RSD) was 2.15%, indicating that the sensor has good reproducibility.

3.5. The specificity of the biosensor

In order to examine the specificity of the sensor, miR-21, single base mismatch, double base mismatch, or complete mismatch sequence at the same concentration or a blank control were added to analyze changes in current values by the DPV method. As shown in Fig. 4A, the highest MB signal and lowest Fc signal were observed after adding miR-21 (curve a), but there were low MB signals and high Fc signals from the single base mismatch (curve b), double base mismatch (curve c), complete mismatch (curve d) and the blank control (curve e). In Fig. 4B, the I_{MB}/I_{Fc} was highest after adding miR-21, while the other

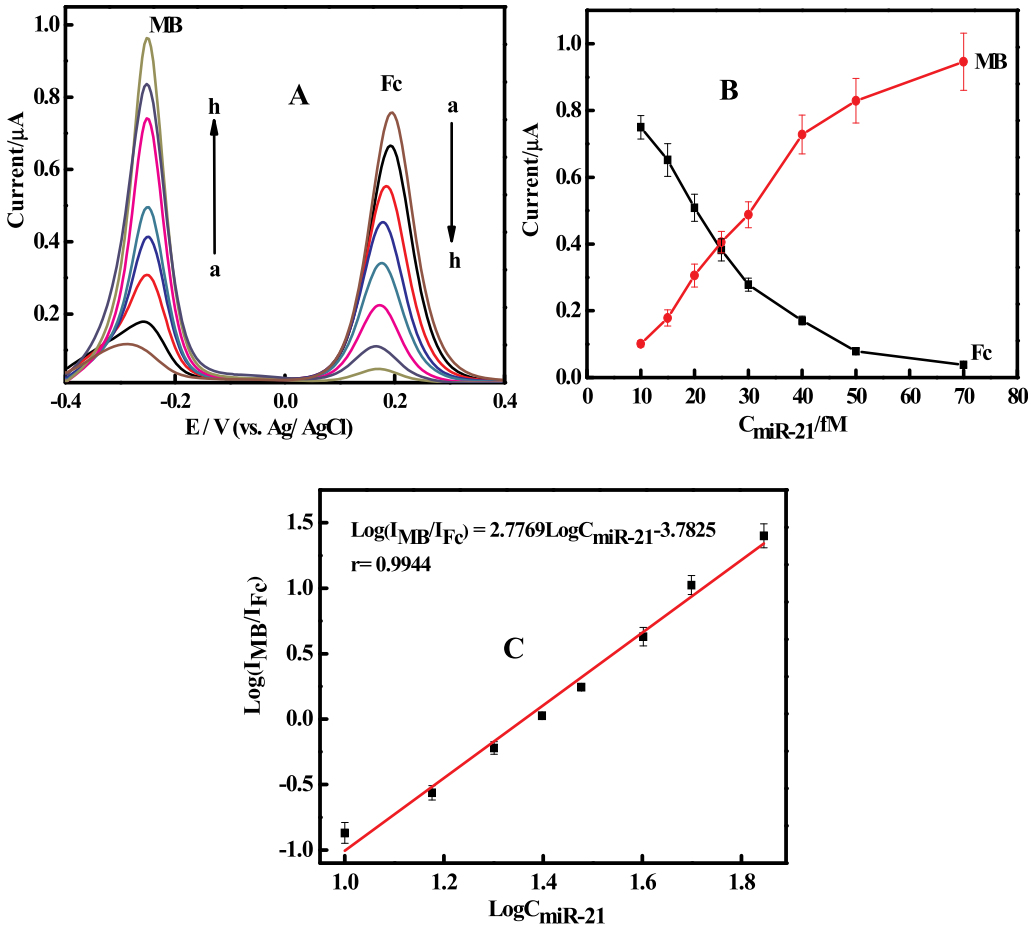

Fig. 3. A. Differential pulse voltammetry curves of "Y" probe-modified glassy carbon electrodes upon addition of miR-21 at different concentrations. B. Current values of "Y" probe-modified glassy carbon electrodes upon addition of miR-21 at different concentrations. C. Calibration plot of Log (I_{MB}/I_{Fc}) versus the logarithm of the miR-21 concentration. MiR-21 concentration (a~h/fM): 10, 15, 20, 25, 30, 40, 50, 70.

signals were almost negligible, indicating that the biosensor demonstrated good selectivity.

3.6. The reproducibility of the biosensor

In order to compare the reproducibility of the ratiometric electrochemical biosensor and the non-ratiometric electrochemical biosensor, 10 samples were detected with the signal on or off sensor, and analysis of variance was conducted. As shown in Fig. 5, the response values had large variations in the single-signal on (Fig. 5A, $\mathbf{\Delta I_{MB}}$) or single-signal off (Fig. 5A, $\mathbf{\Delta I_{Fc}}$) biosensor, and the variances were 0.401 and 0.262, respectively. However, the ratio change of the I_{MB}/I_{Fc} based biosensor (Fig. 5B) had a significantly reduced signal amplitude and the variance was only 0.147. Therefore, the ratiometric electrochemical biosensor has higher reproducibility. Furthermore, the ratiometric electrochemical biosensor has simultaneous "signal-on" (MB) and "signal-off" (Fc) readings, with better stability, reliability and accuracy [33,38].

3.7. Detection of exosomal miR-21 derived from MCF-7

To investigate whether the ratiometric electrochemical biosensor can be used to detect exosomal miR-21, we analyzed the miR-21 level in

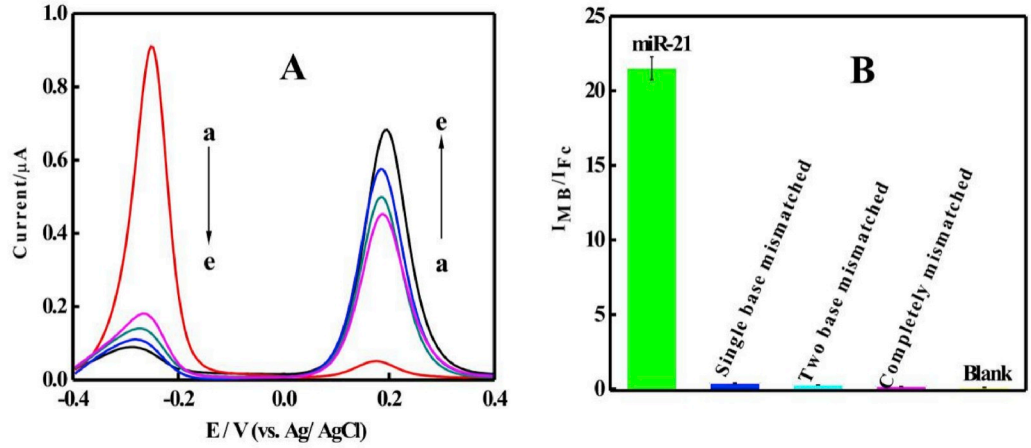

Fig. 4. A. Differential pulse voltammetry curves of "Y" probe-modified glassy carbon electrodes upon addition of miR-21 (a), single base mismatched sequence (b); two base mismatched sequence (c), completely mismatched sequence (d) and the blank control (e). All miRNAs were applied at a 60 fM concentration for the assay. B. I_{MB}/I_{Fc} value of "Y" probe-modified glassy carbon electrodes upon addition of different miRNAs.

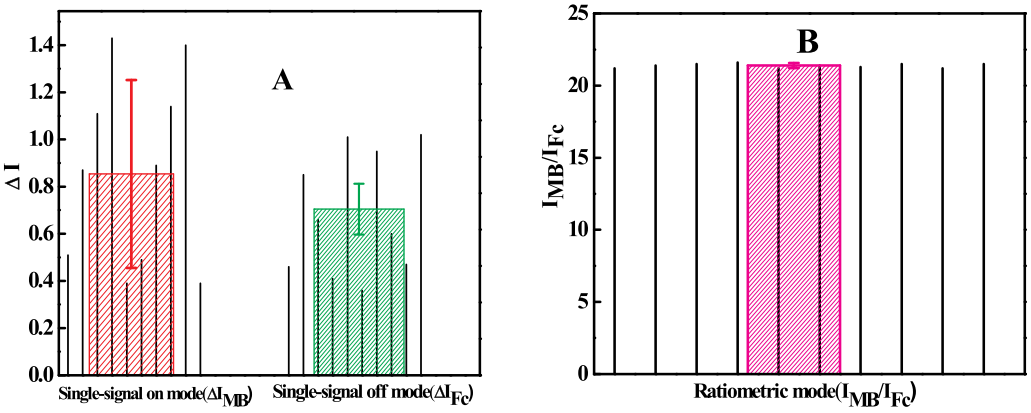

Fig. 5. A. Variance analysis of single-signal on and single-signal off biosensors. B. Variance analysis of the ratiometric biosensor.

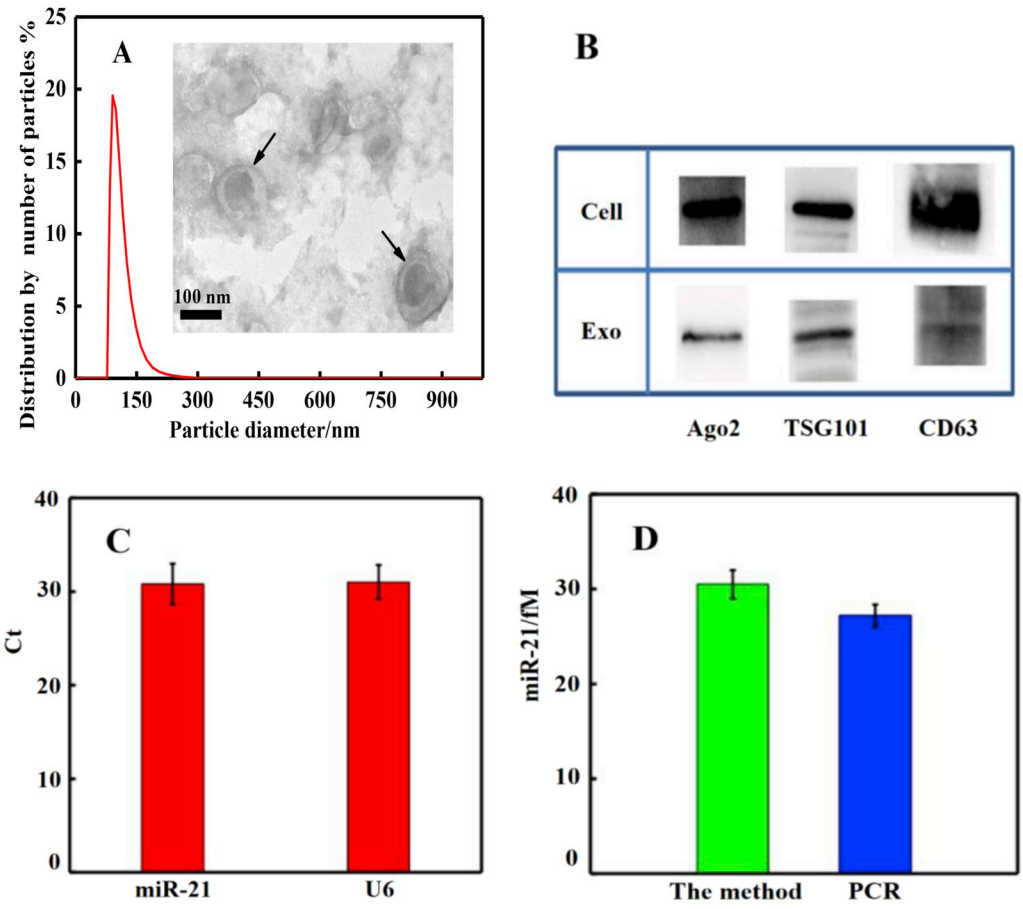

Fig. 6. A. DLS characterization of MCF-7 cell-derived exosomes. Inset: TEM characterization of MCF-7 cell-derived exosomes. B. Western blotting analysis of MCF-7 cell-derivd exosomal proteins. C. Ct values of miR-21 and U6 in MCF-7 cell-derived exosomes. D. Exosomal miR-21 detection by the ratiometric electrochemical biosensor and PCR method.

exosomes derived from breast cancer (MCF-7) cells. According to the International Society for Extracellular Vesicles (ISEV) guidelines [39], exosomes isolated from the supernatant of MCF-7 cells by ultra-centrifugation were characterized. Firstly, the morphology and size of the exosomes were characterized by TEM and DLS. The TEM imaging result (Fig. 6A **inset**) showed that the exosomes were cup-like structure with a particle diameter range of approximately 90–130 nm. Additionally, the DLS result (Fig. 6A) indicated a slightly larger diameter range than that of TEM. This phenomenon can be explained by the fact that the hydro-dynamic diameter of DLS was measured in solution and the exosomes observed by in TEM were likely to have shrunk during the preparation process. Both the results of TEM and DLS agreed with the characteristics of exosomes described in previous literature [26,40]. Then, the exosomal maker proteins Ago2, TSG101 and CD63 were analyzed by western blotting. The obvious bandings in Fig. 6B further confirm the presence of exosomes [41,42]. Next, we extracted miRNA from the exosomes, and analyzed the level of exosomal miR-21 by RT-PCR. As shown in Fig. 6C, the Ct value of miR-21 and U6 snRNA in exosomes were 30.79 and 31.01, respectively, which was similar to those observed in a previous report [43]. Finally, we used our method to determine the content of miR-21 in exosomes, with RT-PCR as a comparison. The detection value of the miR-21 showed no significant difference between two methods (Fig. 6D), indicating that this ratiometric electrochemical biosensor has comparable utility and potential prospects for practical application for the detection of exosomal miR-21.

4. Conclusion

In summary, a biosensor was developed that has merits of electrochemistry, ratiometric readout and simple DNA structural transformation for the sensitive detection of exosomal miR-21 with a LOD as low as 2.3 fM. Compared with single-signal electrochemical sensors, the ratiometric electrochemical biosensor has the advantages of greater stability, reliability and repeatability. Briefly, it has the following features: (1) the application of a "Y" shape-like structure enables the probe to be more stably fixed on the electrode interface; (2) the modification of LNA endows the biosensor with good specificity; and (3) compared with single-signal on and off methods, the dual-signal ratiometric strategy can obtain reliable experimental results, which are less susceptible to the surface state of the electrode, the packing density of the probe, the environment and artificial factors. While the labeled ratiometric electrochemical method requires relatively complicated and high-cost labeling techniques, the construction of a new DNA nanostructure is underway to introduce label-free method for an easier and higher-quality ratiometric electrochemical strategy, even for detecting multiple miRNA markers. Meanwhile, the modification site and quantities of LNA should be optimized for better selectivity and stability of the biosensor. All these endeavors will improve the promising practical application value of the biosensor.

Acknowledgements

The authors gratefully acknowledge the financial support of the National Natural Science Foundation of China (Nos. 21874019), the Natural Science Foundation of Fujian Province (Nos. 2017J07001), the United Fujian Provincial Health and Education Project for Tacking the Key Research P.R. China (WKJ2016-2-30), and the Fujian Science and Technology Innovation Joint Found Project (2016Y9050).

Appendix A. Supplementary data

Supplementary data to this article can be found online at https://doi.org/10.1016/j.talanta.2019.120298.

References

[1] H. Shao, H. Im, C.M. Castro, X. Breakefield, R. Weissleder, H. Lee, New technologies for analysis of extracellular vesicles, Chem. Rev. 118 (4) (2018) 1917–1950.
[2] P. Ziaei, C.E. Berkman, M.G. Norton, Isolation and detection of tumor-derived extracellular vesicles, ACS Appl. Nano Mater. 1 (5) (2018) 2004–2020.
[3] C. Corrado, S. Raimondo, A. Chiesi, F. Ciccia, G. De Leo, R. Alessandro, Exosomes as intercellular signaling organelles involved in health and disease: basic science and clinical applications, Int. J. Mol. Sci. 14 (3) (2013) 5338–5366.
[4] S.N. Tamkovich, O.S. Tutanov, P.P. Laktionov, Exosomes: generation, structure, transport, biological activity, and diagnostic application, Biochem. Suppl. 10 (3) (2016) 163–173.
[5] T. Kadota, Y. Yoshioka, Y. Fujita, T. Ochiya, Exosomes: toward clinical application, Nihon Yakurigaku Zasshi 149 (3) (2017) 119–122.
[6] P. Kucharzewska, H.C. Christianson, J.E. Welch, K.J. Svensson, E. Fredlund, M. Ringnér, M. Mörgelin, E. Bourseau-Guilmain, J. Bengzon, M. Belting, Exosomes reflect the hypoxic status of glioma cells and mediate hypoxia-dependent activation of vascular cells during tumor development, Proc. Natl. Acad. Sci. U.S.A. 110 (18) (2013) 7312–7317.
[7] D.S. Choi, D.K. Kim, Y.K. Kim, Y.S. Gho, Proteomics, transcriptomics and lipidomics of exosomes and ectosomes, Proteomics 13 (10–11) (2013) 1554–1571.
[8] Z. Zeng, Y. Li, Y. Pan, X. Lan, F. Song, J. Sun, K. Zhou, X. Liu, X. Ren, F. Wang, J. Hu, X. Zhu, W. Yang, W. Liao, G. Li, Y. Ding, L. Liang, Cancer-derived exosomal miR-25-3p promotes pre-metastatic niche formation by inducing vascular permeability and angiogenesis, Nat. Commun. 9 (1) (2018) 5395.
[9] T. Fang, H. Lv, G. Lv, T. Li, C. Wang, Q. Han, L. Yu, B. Su, L. Guo, S. Huang, D. Cao, L. Tang, S. Tang, M. Wu, W. Yang, H. Wang, Tumor-derived exosomal miR-1247-3p induces cancer-associated fibroblast activation to foster lung metastasis of liver cancer, Nat. Commun. 9 (1) (2018) 191.
[10] M. Tu, F. Wei, J. Yang, D. Wong, Detection of exosomal biomarker by electric field-induced release and measurement (EFIRM), Biosens. Bioelectron. 44 (2013) 115–121.
[11] G.K. Joshi, S. Deitz-McElyea, T. Liyanage, K. Lawrence, S. Mali, R. Sardar, M. Korc, Label-free nanoplasmonic-based short noncoding RNA sensing at attomolar concentrations allows for quantitative and highly specific assay of microRNA-10b in biological fluids and circulating exosomes, ACS Nano 9 (11) (2015) 11075–11089.
[12] L. Zhu, K. Wang, J. Cui, H. Liu, X. Bu, H. Ma, W. Wang, H. Gong, C. Lausted, L. Hood, Label-free quantitative detection of tumor-derived exosomes through surface plasmon resonance imaging, Anal. Chem. 86 (17) (2014) 8857–8864.
[13] C. Théry, L. Zitvoge, S. Amigorena, Exosomes: composition, biogenesis and function, Nat. Rev. Immunol. 2 (8) (2002) 569–579.
[14] S.A. Melo, L.B. Luecke, C. Kahlert, Glypican-1 identifies cancer exosomes and detects early pancreatic cancer, Nature 523 (7559) (2015) 177–182.
[15] G. Rabinowits, C. Gerçel-Taylor, J.M. Day, Exosomal microRNA: a diagnostic marker for lung cancer, Clin. Lung Cancer 10 (1) (2009) 42–46.
[16] M. Frydrychowicz, A. Kolecka-Bednarczyk, M. Madejczyk, Exosomes-structure, biogenesis and biological role in non-small-cell lung cancer, Scand. J. Immunol. 81 (1) (2015) 2–10.
[17] A. Válóczi, C. Hornyik, N. Varga, J. Burgyán, S. Kauppinen, Z. Havelda, Sensitive and specific detection of microRNAs by northern blot analysis using LNA-modified oligonucleotide probes, Nucleic Acids Res. 32 (22) (2004) e175.
[18] S.D. Fiedler, M.Z. Carletti, L.K. Christenson, Quantitative RT-PCR methods for mature microRNA expression analysis, Methods Mol. Biol. 630 (2010) 49–64.
[19] J. Hu, X. Yue, J. Liu, D. Kong, Construction of an miRNA-gene regulatory network in colorectal cancer through integrated analysis of mRNA and miRNA microarrays, Mol. Med. Rep. 18 (6) (2018) 5109–5116.
[20] H. Cao, X. Zhou, Y. Zeng, Microfluidic exponential rolling circle amplification for sensitive microRNA detection directly from biological samples, Sens. Actuators B Chem. 279 (2019) 447–457.
[21] G.K. Joshi, S. Deitz-McElyea, T. Liyanage, K. Lawrence, S. Mali, R. Sardar, M. Korc, Label-Free nanoplasmonic-based short noncoding RNA sensing at attomolar concentrations allows for quantitative and highly specific assay of microRNA-10b in biological fluids and circulating exosomes, ACS Nano 9 (11) (2015) 11075–11089.
[22] J.U. Lee, W.H. Kim, H.S. Lee, K.H. Park, S.J. Sim, Quantitative and specific detection of exosomal miRNAs for accurate diagnosis of breast cancer using a surface-enhanced Raman scattering sensor based on plasmonic head-flocked gold nanopillars, Small (2019) e1804968.
[23] Y. Pang, C. Wang, L. Lu, C. Wang, Z. Sun, R. Xiao, Dual-SERS biosensor for one-step detection of microRNAs in exosome and residual plasma of blood samples for diagnosing pancreatic cancer, Biosens. Bioelectron. 130 (2019) 204–213.
[24] D. He, L. Hai, H. Wang, R. Wu, H.W. Li, Enzyme-free quantification of exosomal microRNA by the target triggered assembly of polymer DNAzyme nanostructure, Analyst 143 (4) (2018) 813–816.
[25] L.Y. Zhai, M.X. Li, W.L. Pan, Y. Chen, M.M. Li, J.X. Pang, L. Zheng, J.X. Chen, W.J. Duan, In situ detection of plasma exosomal microRNA-1246 for breast cancer diagnostics by a au nanoflare probe, ACS Appl. Mater. Interfaces 10 (46) (2018) 39478–39486.
[26] Y. Xia, L. Wang, J. Li, X. Chen, J. Lan, A. Yan, Y. Lei, S. Yang, H. Yang, J. Chen, Ratiometric fluorescent bioprobe based on carbon dots and acridone derivate for signal amplification detection exosomal microRNA, Anal. Chem. 90 (15) (2018) 8969–8976.
[27] W.A. Hassanain, A. Sivanesan, E.L. Izake, G.A. Ayoko, An electrochemical biosensor for the rapid detection of erythropoietin inblood, Talanta 189 (2018) 636–640.
[28] T. Wang, H. Yin, Y. Zhang, L. Wang, Y. Du, Y. Zhuge, S. Ai, Electrochemical aptasensor for ampicillin detection based on the protective effect of aptamer-antibiotic conjugate towards DpnII and Exo III digestion, Talanta 197 (2019) 42–48.
[29] J. Bao, C. Hou, Y. Zhao, X. Geng, M. Samalo, H. Yang, M. Bian, D. Huo, An enzyme-free sensitive electrochemical microRNA-16 biosensor by applying a multiple signal amplification strategy based on Au/PPy-rGO nanocomposite as a substrate, Talanta 196 (2019) 329–336.
[30] X. Pang, X. Zhang, K. Gao, S. Wan, C. Cui, L. Li, H. Si, B. Tang, W. Tan, Visible light-driven self-powered device based on a straddling nano-heterojunction and bio-application for quantitation of exosomal RNA, ACS Nano 13 (2) (2019) 1817–1827.
[31] K. Boriachek, M. Umer, M.N. slam, V. Gopalan, A.K. Lam, N.T. Nguyen, M.J.A. Shiddiky, An amplification-free electrochemical detection of exosomal miRNA-21 in serum samples, Analyst 143 (7) (2018) 1662–1669.
[32] R. Tavallaie, J. McCarroll, M. Le Grand, N. Ariotti, W. Schuhmann, E. Bakker, R.D. Tilley, D.B. Hibbert, M. Kavallaris, J.J. Gooding, Nucleic acid hybridization on an electrically reconfigurable network of gold-coated magnetic nanoparticles enables microRNA detection in blood, Nat. Nanotechnol. 13 (11) (2018) 1066–1071.
[33] E. Xiong, Z. Li, X. Zhang, J. Zhou, X. Yan, Y. Liu, J. Chen, Triple-helix molecular switch electrochemical ratiometric biosensor for ultrasensitive detection of nucleic acids, Anal. Chem. 89 (17) (2017) 8830–8835.
[34] L. Ge, W. Wang, F. Li, Electro-Grafted electrode with graphene-oxide-like DNA affinity for ratiometric homogeneous electrochemical biosensing of microRNA, Anal. Chem. 89 (21) (2017) 11560–11567.
[35] J. Zhang, L.L. Wang, M.F. Hou, Y.K. Xia, W.H. He, A. Yan, Y.P. Weng, L.P. Zeng, J.H. Chen, A ratiometric electrochemical biosensor for the exosomal microRNAs detection based on bipedal DNA walkers propelled by locked nucleic acid modified toehold mediate strand displacement reaction, Biosens. Bioelectron. 102 (2018) 33–40.
[36] J.M. Obliosca, S.Y. Cheng, Y.A. Chen, M.F. Llanos, Y.L. Liu, D.M. Imphean, D.R. Bell, J.T. Petty, P. Ren, H.C. Yeh, LNA thymidine monomer enables differentiation of the four single-nucleotide variants by melting temperature, J. Am. Chem. Soc. 139 (20) (2017) 7110–7116.
[37] Z. Wen, Q.W. Xia, Q.L. Zhong, J.H. Wen, X.L. He, Electrochemical studies of chloroperoxidase on poly-l-lysine film modified GC electrode, Chin. Chem. Lett. 21 (2010) 93–96.
[38] K. Peng, P. Xie, Z.H. Yang, R. Yuan, K. Zhang, Highly sensitive electrochemical nuclear factor kappa B aptasensor based on target-induced dualsignal ratiometric and polymerase-assisted protein recycling amplification strategy, Biosens.

Bioelectron. 102 (2018) 282–287.
[39] C. Théry, K.W. Witwer, E. Aikawa, et al., Minimal information for studies of extracellular vesicles 2018 (MISEV2018): a position statement of the International Society for Extracellular Vesicles and update of the MISEV 2014 guidelines, J. Extracell. Vesicles 7 (1) (2018) 1535750.
[40] W. Zhang, P. Peng, Y. Kuang, J. Yang, D. Cao, Y. You, K. Shen, Characterization of exosomes derived from ovarian cancer cells and normal ovarian epithelial cells by nanoparticle tracking analysis, Tumour Biol. 37 (3) (2016) 4213–4221.
[41] H. Etayash, A.R. McGee, K. Kaur, Nanomechanical sandwich assay for multiple cancer biomarkers in breast cancer cell-derived exosomes, Nanoscale 8 (33) (2016) 15137–15141.
[42] S.A. Melo, H. Sugimoto, J.T. O'Connell, N. Kato, A. Villanueva, A. Vidal, L. Qiu, E. Vitkin, L.T. Perelman, C.A. Melo, A. Lucci, C. Ivan, G.A. Calin, R. Kalluri, Cancer exosomes perform cell-independent microRNA biogenesis and promote tumorigenesis, Cancer Cell 26 (5) (2014) 707–721.
[43] N.S. Wickramasinghe, T.T. Manavalan, S.M. Dougherty, K.A. Riggs, Y. Li, C.M. Klinge, Estradiol downregulates miR-21 expression and increases miR-21 target gene expression in MCF-7 breast cancer cells, Nucleic Acids Res. 37 (8) (2009) 2584–2595.